JOURNAL OF MATERIALS SCIENCE 28 (1993) 2129–2134

Structure of B_6O boron-suboxide by Rietveld refinement

M. KOBAYASHI, I. HIGASHI
The Institute of Physical and Chemical Research (RIKEN), Wako, Saitama 351-01, Japan
C. BRODHAG, F. THÉVENOT
Ecole Nationale Supérieur des Mines de Saint-Etienne, 158 Cours Fauriel, F42023 Saint-Etienne Cédex 2, France

The structures of the B_6O samples prepared by oxidizing boron with ZnO at temperatures of 1350–1500 °C in an argon atmosphere have been refined by the Rietveld method. The B_6O samples were found to contain an amorphous phase from their X-ray diffraction profiles in addition to B_6O diffraction peaks. The results indicate that the B_6O samples, space group $R\bar{3}m$, no.166, $a_{hex} = 0.5367(1)$ nm and $c_{hex} = 1.2328(2)$ nm in the hexagonal unit cell, have oxygen deficiencies with 0.76(6) oxygen occupancy. A radial distribution function method applied to an extracted portion of the amorphous phase, suggests that each amorphous phase has nearly similar short-range order structure to that of the α-tetragonal boron type rather than to those of any other related boron phases.

1. Introduction

As well as many higher borides comprising B_{12} substructural units, B_6O of the α-rhombohedral boron type has also been investigated because of its ceramic nature (hardness, high melting point, chemical stability, and also low density) as a new structural material [1]. In addition to this, these borides have unique bondings not easily accessible by the usual valence theory [2]. In this regard, much interest has been stimulated regarding their physics and chemistry. Although an X-ray emission spectroscopic method [3] indicated a probable parameter range for the oxygen site of B_6O, the correct oxygen position remained open to question until the Rietveld analyses [4, 5] of X-ray diffraction profiles on B_6O powders were first carried out successfully, even though they were preliminary investigations.

Further X-ray data reductions are reported here related to non-Bragg scatterings, and thickness and background corrections have been made in order to obtain an oxygen occupancy as accurate as possible by the Rietveld refinement.

2. Experimental procedure

2.1. Sample preparation

An "amorphous Moissan boron" containing ~95% B with 0.4% Mg as the main impurity, and powdery ZnO was used. Four samples of B_6O: E3, E4, E6 and E7, were prepared by heating the mixture of boron and zinc oxide [6, 7] at temperatures between 1200 and 1500 °C under an argon atmosphere. Traces of residual zinc metal in the products were leached away using hydrochloric acid. The preparative conditions and properties of the samples are listed in Table I.

2.2. X-ray diffraction and data reduction

Granular samples were gently crushed down in a glass mortar and packed into a non-reflective quartz specimen holder with a well depth of 0.5 mm. X-ray diffraction (XRD) profiles (step scan data for Rietveld refinement) were obtained as described elsewhere [4] through an automated powder X-ray diffractometer (RIGAKU, RAD-IIIB) equipped with a graphite diffracted-beam monochrometer. As the intensity mean counts per second values for 10 s were collected with Cu$K\alpha$ radiation (45 kV, 35 mA) at a step size of 0.05° over a 2θ range 18°–104°. XRD profiles of the samples as measured are shown in Fig. 1. E3, E6 and E7 show XRD patterns mainly of B_6O, but E4 gives one similar to $B_{13}C_2$. Therefore, the description of E4 will be omitted.

Owing to the low linear absorption coefficient of B_6O, $\mu_l = 10.96\ cm^{-1}$, and shallow sample thickness of 0.5 mm, the collected intensity data were corrected for thickness through the following equation [8]

$$I_\infty = I_t[1 - \exp(-2\mu t \operatorname{cosec}\theta)]^{-1} \quad (1)$$

where I_∞ is an intensity corresponding to a specimen of effective infinite thickness, I_t is a collected intensity, μ is the linear absorption coefficient of B_6O multiplied by 0.8 as the ratio of the powder density to that of the solid, and t is the well depth of the specimen holder. Further corrections for asymmetric broadening and displacement of the measured peaks that are encoun-

0022–2461

TABLE I Preparative conditions and properties of B_6O samples

Sample	Preparative conditions[a]		Chemical Composition	Colour[b]
	Temp. (°C)	Time (h)		
E4	1200	9	$B_{10}O$	GB
E3	1350	5	$B_{5.4}O$	DRB
E7	1400	6	$B_{6.6}O$	DRB
E6	1500	4	$B_{5.4}O$	DRB

[a] An argon atmosphere was used.
[b] GB, greyish black; DRB, dark reddish brown.

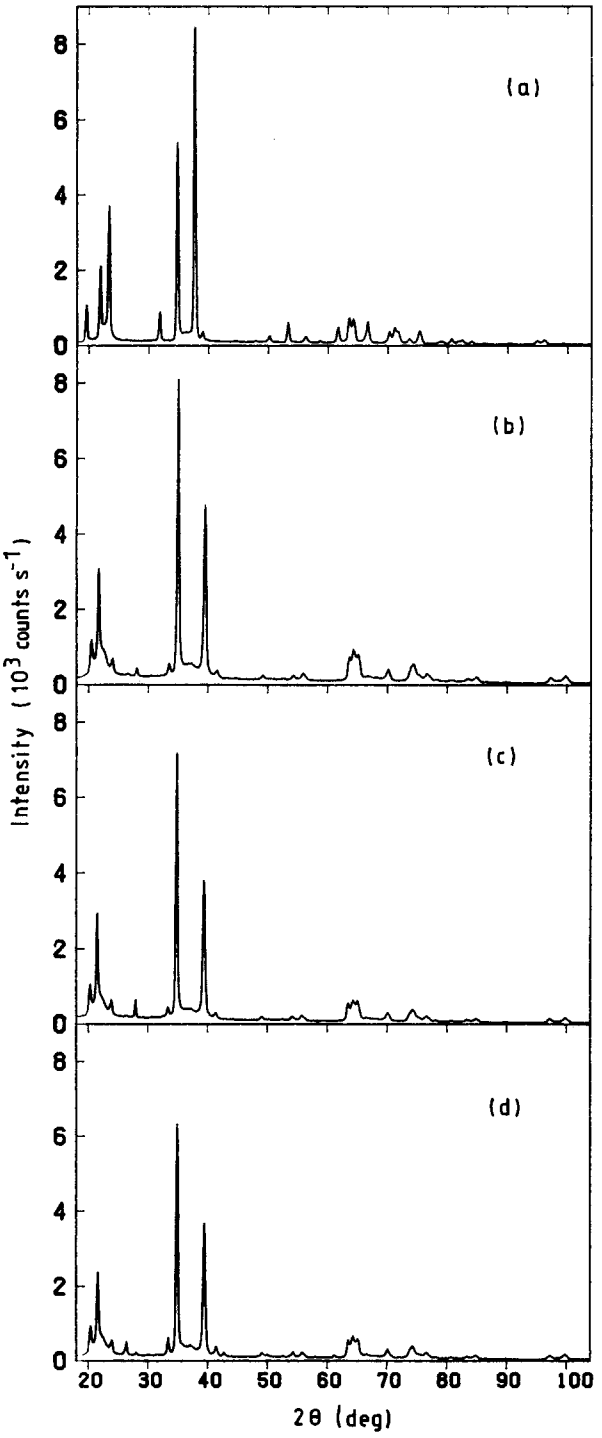

Figure 1 The XRD profiles (Cu$K\alpha$) of the B_6O samples. The reaction temperatures are 1200, 1300, 1400 and 1500 °C, respectively, for (a) E4, (b) E3, (c) E7 and (d) E6 samples. E3, E7 and E6 show XRD patterns ascribed to that of B_6O, but E4 gives one similar to that of $B_{13}C_2$.

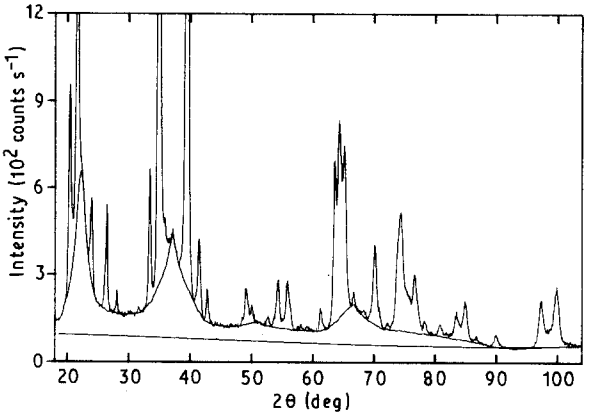

Figure 2 The thickness-corrected observed intensity of specimen E6 where two lines were drawn: one is the line ascribed to the amorphous phase and the other is the estimated background line drawn on the lower side.

tered for a thick specimen with a low absorption coefficient [9] were not considered here for the reasons given above.

For the thickness-corrected intensities, two lines were drawn as depicted in Fig. 2. One is the line traced smoothly along the undulation ascribed to the amorphous phase [7] through visually selected data points excluding Bragg reflection peaks, and the other is the estimated background line which was deduced backwards only, using a polarization factor on the basis of the thickness-corrected intensity at 92° in 2θ where no diffraction peak is observed. Each intensity difference on the data points between the two lines was subtracted from the thickness-corrected intensities that gave the intensity profile data for the Rietveld analysis, although the computer program RIETAN [10] used here is able to cope with an ordinary background, except for large humps due to non-crystalline scatterings on which intense diffraction peaks reside.

3. Results and discussion

3.1. Amorphous phase

As shown in Fig. 1, amorphous or background intensities observed in the XRD patterns decrease in intensity as the reaction temperature increases in the order 1350, 1400 and 1500 °C respectively for E3, E7, and E6 samples. As is evident in Fig. 2, besides the Bragg peaks there exist two large and two small broad humps centred at ~22.2°, ~36.9°, ~50.5°, and ~67.0° in 2θ whose *d*-spacings correspond to 0.40, 0.24, 0.18, and 0.14 nm, respectively. Although these values are close to those for amorphous boron [7], as 0.43, 0.25, 0.17, and 0.14 nm [11], they are not strictly the same. In this regard the structure of the amorphous phase coexisting with crystalline B_6O was suggested to be a packing of B_{12} boron clusters bound with oxygen [7]. The short-range order (SRO) structures of the amorphous phases observed on the reduced RDFs, $G(r)$, are plotted in Fig. 3 in arbitrary units. They were derived by applying an RDF method to the undulation profiles of the amorphous phases extracted

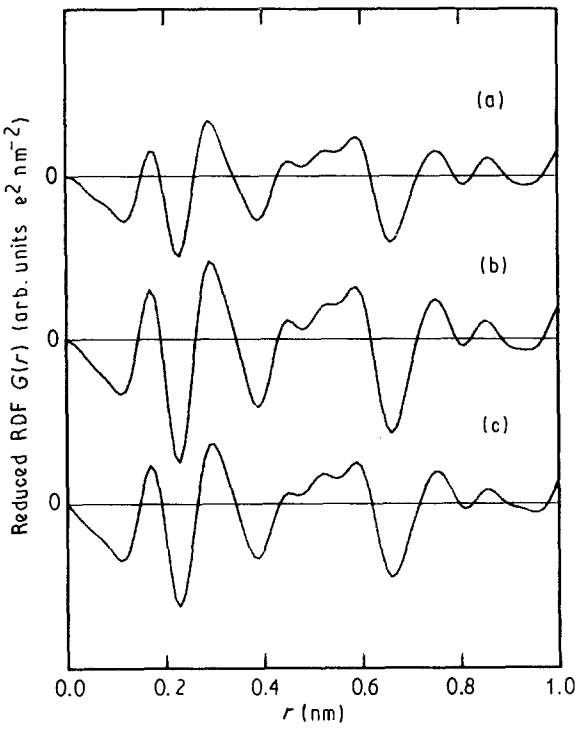

Figure 3 The observed $G(r)_{obs}$ values derived through the RDF method applied to the undulation profiles extracted from the XRD profiles of (a) E3, (b) E7 and (c) E6 samples.

from the XRDs of E3, E7 and E6 specimens. In this case, two extended ranges of XRD profiles were added, both from 3°–18° and 104°–150°, where the step size was doubled to 0.1°. It is seen from the figure that the amorphous phases have nearly the same SRO structure, i.e. they are of the same phase irrespective of their preparative temperatures. Comparison of the $G(r)$ plot with the calculated values unexpectedly reveals that the structure is rather closer to that of the α-tetragonal boron than those of the boron suboxide, B_6O, and of the β-rhombohedral or the amorphous boron used as the raw material. Because the α-tetragonal boron-type compounds are known to exist when impurity atoms such as nitrogen or carbon are present in the reaction system [12], this finding may support the suggestion described above. Further details on this amorphous phase will be submitted elsewhere [13]. Hence the humps or undulations coexisting with the XRD profiles of the B_6O specimens, except E4, are all ascribed to a meaningful amorphous phase. In order to remove such non-Bragg scatterings or an amorphous phase, as observed in the present case, a Fourier-filtering technique has been contrived [14], but the technique does not work well without a structural model properly chosen for the Bragg diffraction peaks whose structure is to be determined.

3.2. Crystalline phase

The Rietveld refinement was made by starting from the previous structural data [4] of B_6O, space group $R\bar{3}m$, no. 166, in a hexagonal unit cell with lattice parameters $a_{hex} = 0.5374(2)$ nm and $C_{hex} = 1.2331(3)$ nm, which stemmed from the structural data of $B_{13}C_2$. In the course of refinement, a full occupancy of the boron sites was assumed, but no preferred orientation was considered due to the hard nature of B_6O which is as hard as adamantine which shows no cleavage planes. Because the specimens used for XRD were not made sufficiently fine for fear of having increased contamination from the glass mortar, some roughness might appear on the surface or flatness, as for the XRD specimen. This generally reduces the observed intensity comparatively in the low 2θ range. In Fig. 1, this tendency can be seen especially in the XRD profile for the E6 sample which was prepared at the highest temperature of all the specimens. Thus it is evident from the figure that the E6 sample has the lowest intensity level of background or amorphous phase. However, each peak intensity or height observed in the low-angle range is not as high as those of E3 and E7 contrary to the expectation that its crystallinity would be the highest. This may partly be due to the differences in the absorption coefficients related to the apparent densities of the specimens. In Table II, the results of the Rietveld refinement, which was applied to the thickness-corrected intensity of E7 by applying individual isotropic thermal parameters, are listed together with the equivalents of E3 which were obtained previously [4]. Because the background level of E7 is rather high compared with that of E6, no amorphous phase extraction was made but the intensity data were excluded from 18°–46° in 2θ as well as in the case of E3, to eliminate the two large humps. It is evident from the table that the cell constant C_{hex} and the atomic coordinates as x, z parameters, are very close within standard deviation, σ. There are, however, large differences in between thermal parameters of B(1) and B(2) atoms indicating different coordination as described below. It should also be noted here that the occupation factors of the oxygen atom site for

TABLE II Atomic coordinates (× 10^3), thermal parameters, site occupancies, and lattice constants of B_6O (space group $R\bar{3}m$, no. 166)

Sample	Atom	Position	x	y	z	B (10^{-2} nm^2)	OCP[a]	a_{hex} (nm)	C_{hex} (nm)
E7	B(1)	18h	153(1)	− x	638(1)	1.2(0.6)	1[b]	0.5362(2)	1.2328(3)
	B(2)	18h	221(1)	− x	779(1)	0.2(0.5)	1[b]		
	0	6c	0	0	624(1)	0.9(1.0)	0.87(13)		
E3 [4]	B(1)	18h	152(2)	− x	638(1)	1.2(0.7)	1[b]	0.5374(2)	1.2331(3)
	B(2)	18h	221(2)	− x	779(1)	0.1(0.6)	1[b]		
	0	6c	0	0	625(1)	1.4(1.2)	0.93(18)		

[a] OCP, occupancy of atom site.
[b] Pre-fixed value.

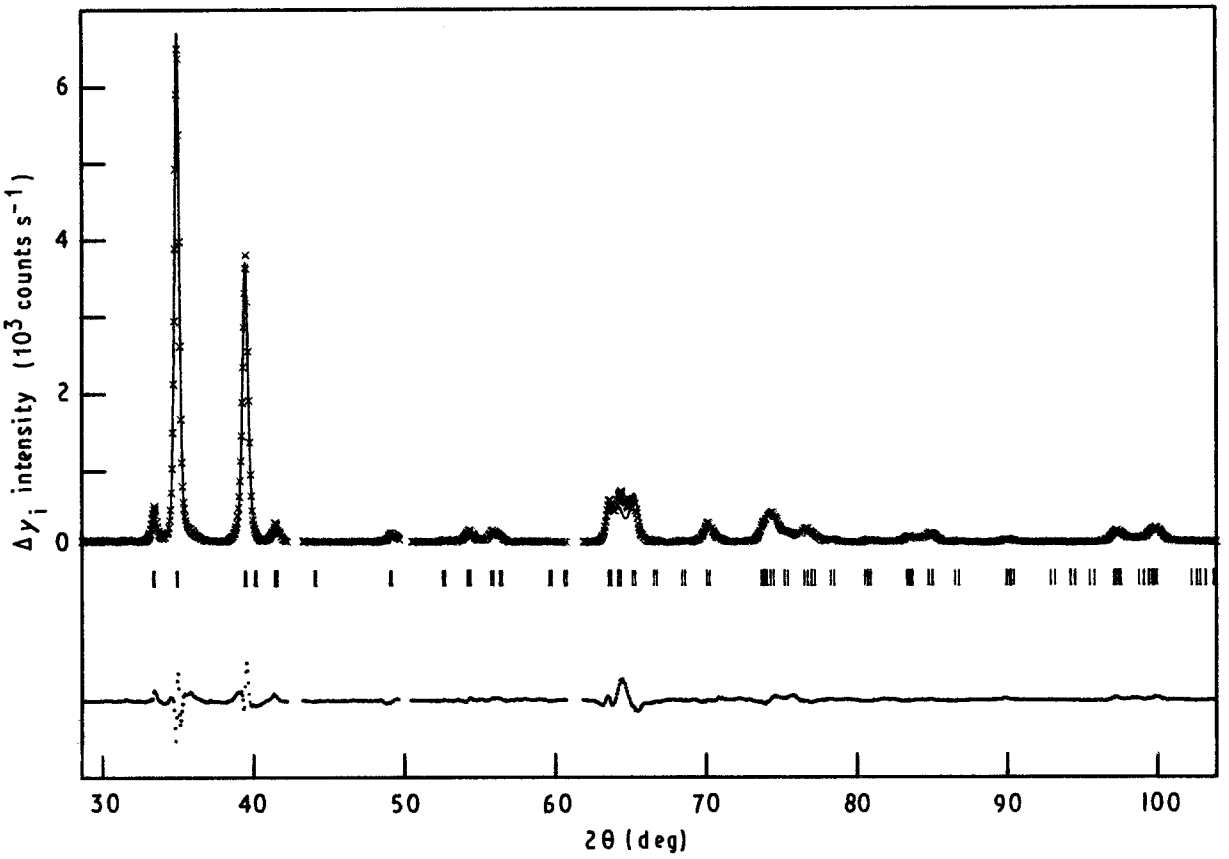

Figure 4 Rietveld refinement patterns for the E6 specimen. The background is subtracted. (—) Calculated intensities; (×) observed intensities; Δy_i, difference between observed and calculated intensities.

TABLE III Atomic coordinates (× 10^3), thermal parameters, site occupancies, and lattice constants of B_6O (space group $R\bar{3}m$, no. 166)

Sample	Atom	Position	x	y	z	$B(10^{-2}$ nm)	OCP[a]	a_{hex}(nm)	C_{hex}(nm)
E6	B(1)	18h	156(2)	$-x$	641(1)	2.4(0.5)	1[b]	0.5367(1)	1.2328(2)
	B(2)	18h	223(1)	$-x$	781(1)	1.5(0.5)	1[b]		
	0	6c	0	0	625(1)	0.1(0.7)	0.76(6)		

[a] OCP, occupancy of atom site.
[b] Pre-fixed value.

both samples are less than unity, as seen in 0.87(13) and 0.93(18) for E7 and E3, although correct values are not yet known. In this respect, a full oxygen occupancy was supposed [4] or assumed [5] in the preceding analyses.

On the contrary, further X-ray data reduction related to the non-Bragg scatterings and background corrections was made for the E6 sample in order to determine the oxygen occupancy as accurate as possible because its XRD profile gave comparatively low-level intensities of background or amorphous phase. As the first step to the Rietveld refinement in this case, common isotropic thermal parameters were applied where only the 2θ range 25°–28.6° was taken out of the data, because an unidentified diffraction peak and a small one of B_2O_3 was observed at around 25.6° and 28°. The structural parameters obtained were then bestowed into the second step where individual isotropic thermal parameters were applied, but followed by a negative one for the oxygen atom. Then, the excluded 2θ range was still made wide, from 18°–28.6°, to exclude the uncertainty originating from tracing along the first large hump and the reason described above. This resulted in a positive thermal parameter for the oxygen atom. Then the intensity data in 2θ regions of 42.3°–43.2°, 49.7°–50.4° and 60.8°–61.8° were further excluded in subsequent refinement because very weak unidentified diffraction peaks were also observed in these regions. The lattice parameters were refined to $a_{hex} = 0.5367(1)$ nm and $c_{hex} = 1.2328(2)$ nm. The reliability indices were $R_{WP} = 14.8\%$, $R_P = 10.7\%$, $R_I = 3.8\%$, and $R_F = 2.8\%$. Fig. 4 illustrates the profile fit and difference patterns for E6 sample. The short vertical lines mark the positions of the possible Bragg peaks (Cu$K\alpha_1$ and Cu$K\alpha_2$). The figure shows that the calculated pattern fits the observed one very well except around 64.5° in 2θ where the observed intensities surpass the calculated ones. This comparatively large difference and others are observed especially around the broad humps, indicating the incorrectly traced undulations of intensities as the amorphous phase. The result is shown in Table III. The values seem to be nearly the same as those in Table II with a slight deviation in

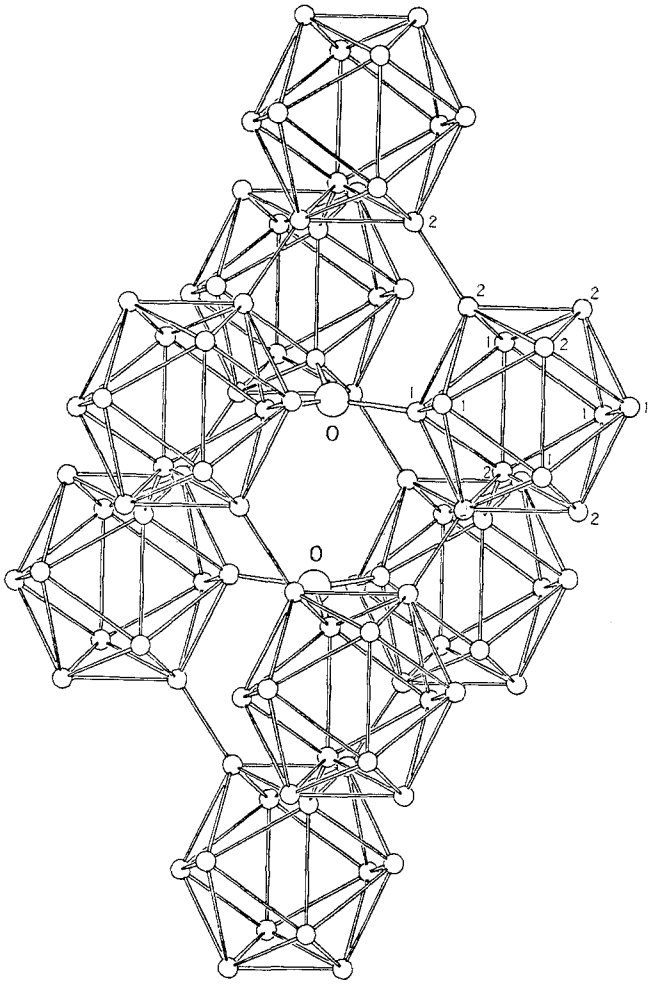

Figure 5 The structure of B_6O. Central large spheres indicate oxygen atoms and small spheres denote boron atoms.

a_{hex}, 0.5367(1) nm, which is, however, almost equal to the average of those of E3 and E7, 0.5368 nm. Therefore, the differences observed here are supposed to be insignificant. It is also seen that the occupancy of the oxygen atom site is less than unity, as found 0.76(6), in contrast to 0.87(13) and 0.93(18) for E7 and E3. However, these values are reconciled to the former one, 0.76(6), if their large σ values are considered.

The calculated density, ρ_{calc}, assuming an occupation factor of 0.76, is estimated to be 2.495 instead of 2.620 g cm^{-3} with full oxygen occupancy, while the observed value, ρ_{obs} = 2.49(1) g cm^{-3}, is obtained by a gradient tube method. The good agreement between ρ_{obs} and ρ_{calc} indicates the validity of the refined values shown in the Table III.

Large differences are also seen in the isotropic thermal parameters of B(1), B(2), and O atoms of which that of the B(1) is the largest. Each oxygen atom located on the [1 1 1] axis of the rhombohedral unit cell makes bonds with neighbouring B(1) atoms of three B_{12} icosahedra, as shown in Fig. 5. In opposition, the B(1) atom is linked with the oxygen atom besides the B(1) and B(2) atoms, so if there is deficiency in the oxygen atom site, some structural strain should be induced around the B(1) atom. Accordingly, an oxygen-deficient site should attribute to the larger thermal parameter for the B(1) atom than for the B(2) atom. In other words, the B(1) atom behaves as in the

TABLE IV Interatomic distances in B_6O samples (nm)

Distance	E3 [4]	E7	E6
B(1)–2B(1)	0.183(2)	0.181(1)	0.177(1)
B(1)–2B(2)	0.180(2)	0.179(2)	0.181(2)
B(1)–B(2)	0.185(3)	0.185(2)	0.184(2)
B(2)–2B(2)	0.181(2)	0.181(1)	0.178(1)
B(2)–B(2) [a]	0.168(2)	0.168(2)	0.166(2)
O–3B(1)	0.143(1)	0.143(1)	0.146(1)
O–O	0.308(2)	0.305(2)	0.307(2)

[a] An intericosahedral distance.

static disorder state, as observed for AlB_{31} [15] and Al–Cu–B_{105} [16] crystals, while the thermal parameter of this constrained oxygen atom is small compared to that of the B(1) atom. In this regard, further Rietveld refinement in applying anisotropic thermal parameters was also attempted in vain, due to insufficient accuracy in the observed intensity data.

Interatomic distances in B_6O samples of E3, E7 and E6 are listed in Table IV where no large differences are seen except that of B(1) and B(1) atoms. However, this difference is not significant, because a similar trend in figures was found when the 2θ range excluded was wide, similar to that of E3 and E7. The distance between oxygen atoms on the [1 1 1] rhombohedral axis is found here again to be 0.307(2) nm which is much longer than that of the oxygen molecule, indicating little interaction between them [3, 4].

In order to confirm the presently observed oxygen-deficient structure of B_6O, however, further detailed study is required on B_6O powders containing no impurities or amorphous phase, or otherwise on a single crystal of good quality.

4. Conclusions

The oxygen-deficient structures of the B_6O samples (space group $R\bar{3}m$, no. 166) were revealed by Rietveld analysis. The oxygen occupation factor in the structure was suggested to be around 0.76(6). The unit cell dimensions were refined to be a_{hex} = 0.5367(1) nm and c_{hex} = 1.2328(2) nm in the hexagonal unit cell. The R factors obtained were R_{WP} = 14.8%, R_P = 10.7%, R_I = 3.8%, and R_F = 2.8%, respectively.

Acknowledgement

The authors thank Dr F. Izumi for supplying the RIETAN program for the Rietveld analysis which was used in this experiment.

References

1. H. F. RIZZO, W. C. SIMMONS, and H. O. BIELSTEIN, *J. Electrochem. Soc.* **109** (1962) 1079.
2. I. HIGASHI, in "Boron Rich Solids", AIP Conference no. 140, Proceedings of the International Conference on the Physics and Chemistry of Boron and Boron-Rich Solids 1985, Albuquerque, New Mexico, USA, edited by D. Emin, T. Aselage, C. L. Beckel, I. A. Howard, and C. Wood (AIP, New York, 1986) pp. 1–10.

3. J. KAWAI, K. MAEDA, I. HIGASHI, M. TAKAMI, Y. HAYASHI and M. UDA, *Phys. Rev. B* **42** (1990) 5693.
4. I. HIGASHI, M. KOBAYASHI, J. BERNHARD, C. BRODHAG and F. THÉVNOT, in "Boron Rich Solids", AIP Conference no. 231, Proceedings of the 10th International Symposium of Boron, Borides, and Related Compounds 1990, Albuquerque, New Mexico, USA, edited by D. Emin, T. Aselage, A. Switendick, B. Morgan and C. Beckel (AIP, New York, 1991) pp. 201–4.
5. H. BOLMGREN and T. LUNDSTRÖM, *ibid.*, pp. 197–200.
6. C. F. HOLCOMBE Jr, and O. J. HORNE Jr, *J. Amer. Ceram. Soc.* **55** (1972) 106.
7. C. BRODHAG and F. THÉVENOT, *J. Less-Common Metals* **117** (1986) 1.
8. H. P. KLUG and L. E. ALEXANDER, in "X-Ray Diffraction Procedures For Polycrystalline and Amorphous Materials", 2nd Edn (Wiley, New York, 1974) p. 360.
9. D. T. KIETING and B. E. WARREN, *Rev. Sci. Instrum.* **23** (1952) 519.
10. F. IZUMI, *Nippon Kessyo Gakkaishi* (*J. Crystallogr. Soc. Jpn*) **27** (1985) 23.
11. M. KOBAYASHI, *J. Mater. Sci.* **23** (1988) 4392.
12. E. AMBERGER and K. PLOOG, *J. Less-Common Metals* **23** (1971) 21.
13. M. KOBAYASHI, I. HIGASHI, C. BRODHAG and F. THÉVENOT to be submitted.
14. J. V. RICHARDSON Jr and J. FABER Jr, in "Advance in X-ray Analysis", vol. 29, Proceedings of the 34th Annual Conference on Application of X-Ray Analysis, Snowmass, August 1985, edited by C. S. Barrett, J. B. Cohen, J. Faber Jr, R. Jenkins, D. E. Leyden, J. C. Russ and P. K. Predecki (Plenum Press, New York, 1956) p. 143.
15. I. HIGASHI, H. IWASAKI, T. ITO, T. LUNDSTRÖM, S. OKADA and L. E. TERGENIUS, *J. Solid State Chem.* **82** (1989) 230.
16. I. HIGASHI, M. KOBAYASHI, Y. AKAGAWA, K. KOBAYASHI and J. BERNHARD, in "Boron Rich Solids", AIP Conference no. 231, Proceedings of the 10th International Symposium of Boron, Borides, and Related Compounds 1990, Albuquerque, New Mexico, USA, edited by D. Emin, T. Aselage, A. Switendick, B. Morgan and C. Beckel (AIP, New York, 1991) pp. 224–31.

Received 5 November 1991
and accepted 14 August 1992